

Dynamics of Nuclear Polarization in InGaAs Quantum Dots in a Transverse Magnetic Field

S. Yu. Verbin^{a,b,*}, I. Ya. Gerlovin^a, I. V. Ignatiev^{a,b,**}, M. S. Kuznetsova^{a,b},
R. V. Cherbunin^{a,b}, K. Flisinski^b, D. R. Yakovlev^{b,c}, and M. Bayer^{b,***}

^aSpin Optics Laboratory, St. Petersburg State University, St. Petersburg, 198504 Russia

^bTechnische Universität Dortmund, 44227 Dortmund, Germany

^cIoffe Physicotechnical Institute, Russian Academy of Sciences, St. Petersburg, 194021 Russia

*e-mail: syuv54@mail.ru

**e-mail: ivan_ignatiev@mail.ru

Received July 24, 2011

Abstract—The time-resolved Hanle effect is examined for negatively charged InGaAs/GaAs quantum dots. Experimental data are analyzed by using an original approach to separate behavior of the longitudinal and transverse components of nuclear polarization. This made it possible to determine the rise and decay times of each component of nuclear polarization and their dependence on transverse magnetic field strength. The rise and decay times of the longitudinal component of nuclear polarization (parallel to the applied field) were found to be almost equal (approximately 5 ms). An analysis of the transverse component of nuclear polarization shows that the corresponding rise and decay times differ widely and strongly depend on magnetic field strength, increasing from a few to tens of milliseconds with an applied field between 20 and 100 mT. Current phenomenological models fail to explain the observed behavior of nuclear polarization. To find an explanation, an adequate theory of spin dynamics should be developed for the nuclear spin system of a quantum dot under conditions of strong quadrupole splitting.

DOI: 10.1134/S1063776112040176

1. INTRODUCTION

Nuclear spin orientation, or dynamic nuclear polarization (DNP), in solids has been extensively investigated since the middle of the past century [1]. The dominant DNP mechanism in semiconductors is the angular momentum transfer from optically oriented electrons to nuclei via electron–nucleus hyperfine interaction [2]. This process is particularly effective in quantum-dot heterostructures, where the electron wavefunction covers a limited number of nuclei, and electron and nuclear spins make up a strongly coupled system. Since spin-polarized nuclei, in turn, generate an effective magnetic field acting on electrons (Overhauser field), the state of the nuclear system can be examined by optical spectroscopic methods. Nuclear spin dynamics in semiconductors was extensively investigated during the last three decades [2, 3]. In bulk semiconductors and quantum wells, nuclear spin relaxation times were found to be a few seconds or longer [4]. First measurements, reported in recent years, have shown that nuclear spin relaxation in quantum dots is much faster. In particular, nuclear spin relaxation in a magnetic field applied parallel to the optical axis (longitudinal field) was found to occur over times on the order of milliseconds [5–8].

Dynamic nuclear polarization in quantum dots in a magnetic field perpendicular to the optical axis (in Voigt geometry) has not been studied until recently. An applied transverse magnetic field reduces the degree of circular polarization of luminescence from semiconductors (Hanle effect) because of the photo-induced precession of electron (or exciton) spins in the field. The effective field generated by spin-polarized nuclei can drastically change the shape of the Hanle curve [2, 9, 10]. This provides an opportunity to examine the dynamics of nuclear polarization experimentally by performing time-resolved measurements of the Hanle effect.

The first observations of the time-resolved Hanle effect in an ensemble of negatively charged InGaAs/GaAs quantum dots [11] demonstrated that experiments of this kind would provide an effective tool for examining dynamics of a nuclear spin system. In this paper, systematic experimental data presented and analyzed to estimate the nuclear polarization buildup and decay times for the structure under study. In our experiments, we used intensity-modulated optical pumping with various dark and excitation times, t_d and t_{exc} .

The Hanle curves obtained under strong pumping for the sample under study are largely similar in shape to those observed previously for donor-bound elec-

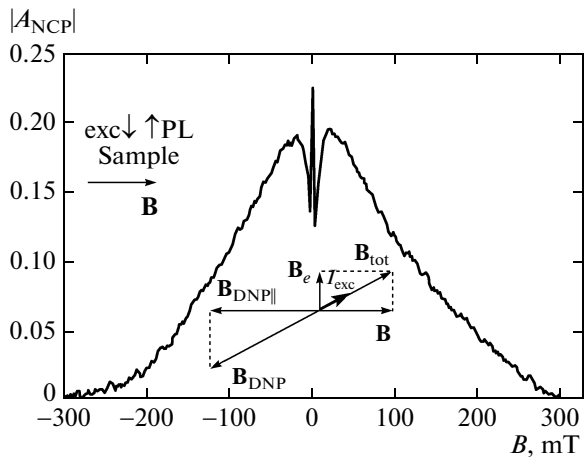


Fig. 1. Degree of luminescence polarization vs. transverse magnetic field (Hanle curve) under CW pumping with excitation intensity $I_{\text{exc}} = 40 \text{ W/cm}^2$. The inserts on the left and at the bottom schematize, respectively, the experimental geometry and the formation of the effective nuclear field \mathbf{B}_{DNP} acting on the electron spin (see text for details); PL = photoluminescence.

trons, in qualitative agreement with predictions of a classical model of DNP in a transverse magnetic field [2, 3]. However, the classical model fails to explain an increase in Hanle curve width with optical pumping intensity observed in our experiments. Following [11, 12], we suppose that the Hanle curve broadening is due to nuclear polarization stabilized by quadrupole splitting of nuclear spin states. An analysis of time-resolved measurement data provides quantitative estimates of the rise and decay times for longitudinal and transverse nuclear fields in the structures under study.

2. EXPERIMENTAL DETAILS

We examined a heterostructure containing 20 layers of self-assembled InGaAs/GaAs quantum dots separated by n -doped GaAs barriers. The doping level was adjusted to have an average of one electron per dot. The interaction time between such electrons and nuclei is not limited by their recombination time with photogenerated holes, which should facilitate creating a significant nuclear polarization. The structure was annealed at 900°C to partially reduce stresses in the quantum dots via mutual diffusion of Ga and In atoms. We measured the degree of circular polarization of photoluminescence as a function of magnetic field (Hanle curve).

Luminescence was excited with a continuous-wave Ti:Sapphire laser at frequencies corresponding to optical transitions in the wetting layer. To study dynamics of nuclear polarization, we used a square-wave intensity-modulated beam of constant circular polarization. Laser intensity was modulated with an acousto-optic modulator to produce pulses with various excita-

tion and dark times. The radiation emitted by the sample was passed through a monochromator and detected at the quantum-dot photoluminescence band maximum by means of a single-photon counting avalanche photodiode.

Degree of polarization was measured by using a standard technique where light is passed through a photoelastic modulator and a polarization analyzer. The modulator creates a sinusoidally varying phase shift between linearly polarized beam components, $\Delta\phi = (\pi/4)\sin(2\pi ft)$ with $f = 50 \text{ kHz}$, thus converting each circularly polarized (σ^+ and σ^-) component of luminescence into linearly polarized (x and y) components. The pulses generated by the photodiode were accumulated by one of two methods. In one of these, a two-channel photon counter was used to measure the luminescence intensity detected by each channel within narrow time gates of $2.5 \mu\text{s}$ around the extrema of $\Delta\phi$. In the other, a FAST ComTec multiscaler card (time-of-flight analyzer) was used to record the time-dependent luminescence detected after a pump pulse had arrived. Since the gate width was usually set to $1 \mu\text{s}$, the signal produced by the photoelastic modulator and analyzer was a sine wave superimposed on a constant background. The signal was processed to compute time-dependent circular polarization of luminescence.

The quantum dots were negatively polarized; i.e., luminescence was predominantly σ^- polarized when excited by a σ^+ -polarized beam [6]. The mechanism responsible for negative circular polarization (NCP) has been widely discussed in the literature [13–15]. NCP was shown to result from optically induced spin orientation of the resident electron. The amplitude of circular polarization is proportional to the projection of electron spin on the optical axis (z axis) averaged over an ensemble of quantum dots [15]:

$$A_{\text{NCP}} \propto 2 \langle S_z \rangle. \quad (1)$$

This implies that the absolute value of the amplitude can be used to quantify the degree of electron spin orientation. The key factor that determines the orientation of an electron spin in a quantum dot is its hyperfine interaction with nuclear spins [2]. Therefore, analysis of electron spin dynamics can provide information about nuclear spin orientation.

The Hanle curve measured under continuous-wave (CW) pumping is W shaped with a narrow central peak (Fig. 1), indicating the occurrence of DNP [2, 9]. When the excitation pulse is sufficiently long ($t_{\text{exc}} > 50 \text{ ms}$), the shape of the Hanle curve is almost identical to that observed under CW pumping. In other words, the state of the electron–nuclear system at the end of pumping is independent of its previous dynam-

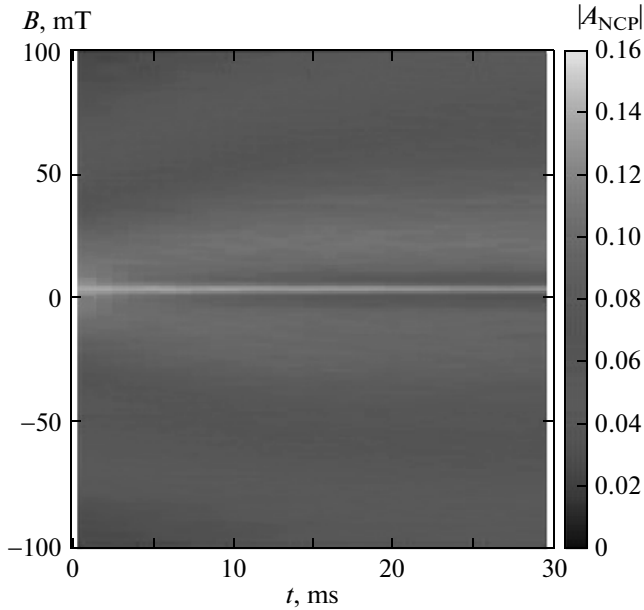


Fig. 2. Degree of polarization measured as a function of magnetic field B and time after the start of pumping (the grayscale bar on the right indicates $|A_{\text{NCP}}|$ intensity).

ics (in particular, the dark time between pulses). The shape of the Hanle curve changes with modulation parameters.

3. EXPERIMENTAL RESULTS

To examine nuclear polarization buildup, we used the multichannel photon counting system described above to measure NCP as a function of time after a

pump pulse had arrived. Figure 2 demonstrates the change in shape of the Hanle curve with time elapsed after the start of pumping. Immediately after the start of pumping, the Hanle curve is smooth and narrow. The curve widens with time elapsed, and dips appear around the central peak; i.e., a W profile develops. Both W-profile width and dip depth reach maximum values under CW pumping.

Nuclear spin relaxation was examined by detecting luminescence during a short interval $t_{\text{det}} = 1$ ms at the start of pumping after various dark times. Pumping was supposed to have a weak effect on nuclear polarization during the detection time. The degree of polarization was measured as a function of dark time by varying t_d from 20 μs to 50 ms. Figure 3a shows the Hanle curves obtained for several dark times, and Fig. 3b shows their central portions. It is clear that the curves corresponding to short dark times are similar to that obtained under CW pumping (see Fig. 1). In particular, a pronounced W profile is observed, and the curve is wider. An increase in dark time smoothes out the W profile and reduces the width of the Hanle curve.

Our experimental findings suggest that the development of nuclear polarization generally leads to a decrease in electron spin polarization in weak transverse magnetic fields and its increase in strong fields. It is obvious that these effects are associated with two different processes.

According to the model proposed in [9], based on the concept of spin temperature [16], a W profile develops in the Hanle curve under strong pumping because of a significant DNP parallel to the total field \mathbf{B}_{tot} affected the nuclear spins. This field is the sum of the applied field \mathbf{B} and the effective field B_e generated by optically oriented electrons (Knight field). As the

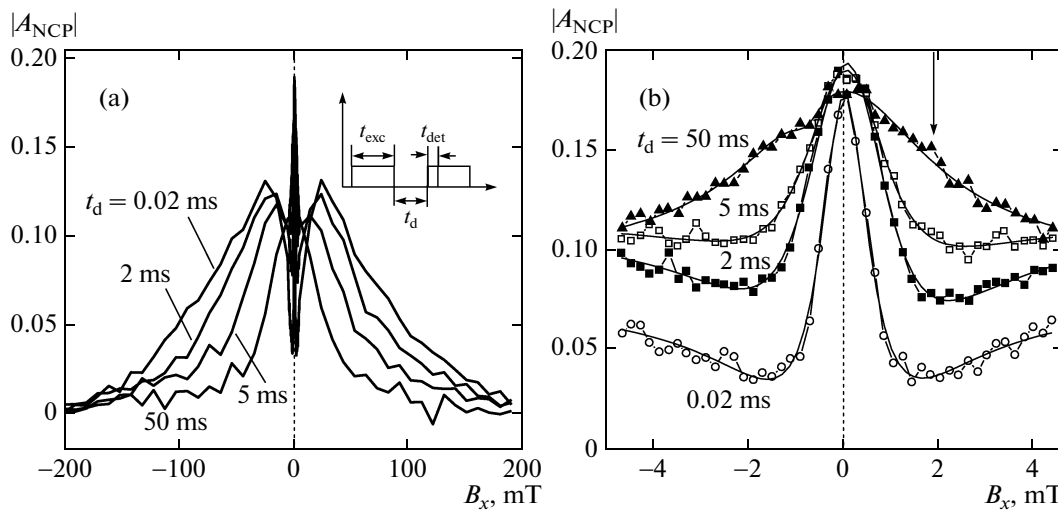


Fig. 3. Hanle curves at constant excitation time $t_{\text{exc}} = 100$ ms and intensity $I_{\text{exc}} = 40$ W/cm², parameterized by dark time t_d (indicated at each curve): (a) complete curves; (b) central portions of curves. The arrow points to the lowest point of a dip in a Hanle curve. The solid curves are drawn for clarity.

applied field exceeds the Knight field, the total field and, accordingly, the nuclear field begin to rotate away from the optical axis towards the applied field direction. The rotation reduces the degree of electron spin polarization, resulting in a weaker Knight field. This, in turn, additionally increases the angle of rotation. In effect, positive feedback of this kind leads to the formation of a narrow central peak in the Hanle curve.

The effective nuclear magnetic field acting on an electron spin in the system under study is parallel to the nuclear spin direction [2, 3]. When the applied magnetic field is weak (in the dip region around the central peak), the nuclear field is stronger than the applied one, and the electron spin is effectively depolarized by a high \mathbf{B}_{tot} . Nuclear field decreases with increasing applied field, and the ensuing increase in electron spin polarization leads to the development of a W profile in the Hanle curve. This implies that dynamics of the longitudinal component $\mathbf{B}_{\text{DNP}\parallel}$ of nuclear field can be inferred from the time evolution of the dips around the central peak. Note that the terms *longitudinal* and *transverse* used in the present study refer, respectively, to the nuclear field components parallel and perpendicular to the applied magnetic field (as in [16]) rather than the optical axis (e.g., see [2]).

Information about behavior of the transverse component $\mathbf{B}_{\text{DNP}\perp}$ of nuclear field can be extracted by analyzing the width of the Hanle curve. It is clear from Figs. 2 and 3 that the curve width reaches a maximum under CW pumping by a beam of constant circular polarization and decreases with increasing dark time when the pump beam is modulated. Its large width has been attributed to the formation of a transverse component $\mathbf{B}_{\text{DNP}\perp}$ of nuclear field stabilized by quadrupole splitting of nuclear spin states along the optical axis [11, 12]. Since the longitudinal component $\mathbf{B}_{\text{DNP}\parallel}$ plays no significant role in strong applied magnetic fields [2, 3], dynamics of $\mathbf{B}_{\text{DNP}\parallel}$ and $\mathbf{B}_{\text{DNP}\perp}$ can be inferred separately from behavior of electron spin polarization in weak and strong fields, respectively. Accordingly, to analyze experimental data, expressions are required that relate the degree of electron polarization to the magnitudes of the corresponding DNP components.

4. ANALYSIS OF EXPERIMENTAL DATA

4.1. Formulas for Analysis

To derive expressions for nuclear spin components, we can reasonably assume that the only time-invariant component of electron spin is its projection on \mathbf{B}_{tot} because of its high precession frequency. Measured degree of luminescence polarization scales linearly with the invariant spin projection on the viewing direction,

$$S_z = S \cos^2 \vartheta = S \frac{B_{\text{tot},z}^2}{B_{\text{tot}}^2}, \quad (2)$$

where S quantifies the degree of optically induced spin orientation and ϑ is the angle between the viewing direction and the total field $\mathbf{B}_{\text{tot}} = \mathbf{B} + \mathbf{B}_{\text{N}}$ (the sum of the applied field \mathbf{B} and the nuclear field $\mathbf{B}_{\text{N}} = \mathbf{B}_{\text{f}} + \mathbf{B}_{\text{DNP}}$ including the effective nuclear spin fluctuation field generated by randomly oriented nuclear spins [17]). Since the electron spin in a quantum dot interacts with just a few nuclear spins, the contribution due to fluctuations is significantly larger than that for donor-bound electron spins in a bulk material, amounting to several tens of milliteslas [18]. Therefore, we can evaluate only an ensemble-averaged spin $\langle S_z \rangle$.

In the absence of regular fields \mathbf{B} and \mathbf{B}_{DNP} , electron spin dynamics is completely determined by nuclear spin fluctuations. A magnetic field applied perpendicular to the optical axis (hereinafter assumed parallel to the x axis) substantially changes the time-averaged electron spin polarization. It was shown in [17] that rigorous evaluation of S_z is a cumbersome task. The calculated field dependence of S_z can be described by a bell-shaped curve accurately fitted by (2) with

$$B_{\text{tot},z}^2 = \langle B_{f,z}^2 \rangle,$$

where $\langle B_{f,z}^2 \rangle$ is the ensemble average of the nuclear spin fluctuation field z component squared and

$$B_{\text{tot}}^2 = B^2 + \langle B_f^2 \rangle,$$

with $\langle B_f^2 \rangle = \langle B_{f,x}^2 \rangle + \langle B_{f,y}^2 \rangle + \langle B_{f,z}^2 \rangle$. Thus, the mean ratio approximated by the ratio of means in (2),

$$\langle S_z \rangle \approx S \frac{\langle B_{\text{tot},z}^2 \rangle}{\langle B_{\text{tot}}^2 \rangle}, \quad (3)$$

yields a satisfactory result under conditions specified above.

We suppose that approximation (3) holds in the presence of a regular field \mathbf{B}_{DNP} , with a periodically time-varying numerator:

$$B_{\text{tot},z} = B_{\text{N}\perp} \cos \omega t,$$

where $B_{\text{N}\perp}$ is the component of the total nuclear field perpendicular to the applied field and ω is the frequency of nuclear spin precession induced by the applied field. The electron pumping rate was higher than the nuclear precession frequency in the entire range of applied magnetic field magnitudes used in the experiments described here. Therefore, we can represent the numerator in (3) as

$$\begin{aligned} \langle B_{\text{tot},z}^2 \rangle &= (B_{\text{DNP}\perp}^2 + \langle B_{f\perp}^2 \rangle) \langle \cos^2 \omega t \rangle \\ &= 0.5(B_{\text{DNP}\perp}^2 + \langle B_{f\perp}^2 \rangle), \end{aligned} \quad (4)$$

where

$$\langle B_{f\perp}^2 \rangle = \langle B_{f,z}^2 \rangle + \langle B_{f,y}^2 \rangle = 2 \langle B_{f,x}^2 \rangle \equiv 2 \langle B_{f\parallel}^2 \rangle.$$

Analogously, the ensemble average of the total field squared (denominator in (3)) can be expressed as

$$\langle B_{\text{tot}}^2 \rangle = (B + B_{\text{DNP}\parallel})^2 + \langle B_{f\parallel}^2 \rangle + B_{\text{DNP}\perp}^2 + \langle B_{f\perp}^2 \rangle. \quad (5)$$

In summary, the degree of electron spin polarization can be represented by the general expression

$$\rho = \frac{\langle S_z \rangle}{S} = \frac{0.5(B_{\text{DNP}\perp}^2 + \langle B_{f\perp}^2 \rangle)}{(B + B_{\text{DNP}\parallel})^2 + B_{\text{DNP}\perp}^2 + \langle B_{f\perp}^2 \rangle}, \quad (6)$$

where

$$\langle B_f^2 \rangle = \langle B_{f\parallel}^2 \rangle + \langle B_{f\perp}^2 \rangle = 3\langle B_{f\parallel}^2 \rangle.$$

The last relation holds when dynamic nuclear polarization is insignificant and nuclear spin fluctuations are statistically isotropic.

According to (6), the degree of electron spin polarization approaches 1/3 as $B \rightarrow 0$ and in the absence of DNP, in full agreement with [17]. Actual measurements show that it is approximately 1.5 times lower when DNP does not develop because of a fast pump polarization modulation. In our view, the lower degree of electron spin polarization is due to the unpolarized luminescence from neutral quantum dots contributing to the recorded signal.

Experimental data can be analyzed by simplifying expression (6) in two special cases of particular importance. According to [2], the longitudinal component $B_{\text{DNP}\parallel}$ of nuclear field appears only in the W-profile region of the Hanle curve, where the applied field is negligible compared to the nuclear spin fluctuation field [17]. Then, it holds for this region that

$$\rho \approx \frac{0.5(B_{\text{DNP}\perp}^2 + \langle B_{f\perp}^2 \rangle)}{(B_{\text{DNP}\parallel})^2 + B_{\text{DNP}\perp}^2 + 3\langle B_{f\parallel}^2 \rangle}. \quad (7)$$

In strong applied magnetic fields (as $B_{\text{DNP}\parallel} \rightarrow 0$), the degree of polarization becomes

$$\rho \approx \frac{0.5(B_{\text{DNP}\perp}^2 + \langle B_{f\perp}^2 \rangle)}{B^2 + B_{\text{DNP}\perp}^2 + 3\langle B_{f\parallel}^2 \rangle}. \quad (8)$$

Thus, we can examine the time dependence of ρ in strong and weak magnetic fields to determine the respective kinetics of the longitudinal and transverse components of nuclear polarization.

Our analysis of time-dependent nuclear polarization is based on the assumption that the increase in each component of nuclear polarization after the start of pumping and its decay during the dark time can be described by the expressions

$$y = B_{\text{DNP}}^0 [1 - \exp(-t/\tau)]$$

and

$$y = B_{\text{DNP}}^0 \exp(-t/\tau),$$

where τ is the corresponding characteristic time, respectively. In the case of a weak magnetic field, we

divide the numerator and denominator in (7) by $\langle B_{f\parallel}^2 \rangle$ and introduce

$$a^2 = \frac{(B_{\text{DNP}\perp}^0)^2}{\langle B_{f\parallel}^2 \rangle}$$

and

$$c^2 = \frac{(B_{\text{DNP}\parallel}^0)^2}{\langle B_{f\parallel}^2 \rangle}$$

to find respective expressions describing the rise and decay of the longitudinal component of nuclear polarization:

$$\rho \approx \frac{0.5a^2 + 1}{c^2(1 - e^{-t/\tau})^2 + a^2 + 3} \quad (9)$$

and

$$\rho \approx \frac{0.5a^2 + 1}{c^2 e^{-2t/\tau} + a^2 + 3}. \quad (10)$$

In what follows, we show that the transverse component of nuclear polarization almost vanishes in weak magnetic fields, and the parameter a can be neglected in analysis of experimental data. For this reason time dependence of this parameter is omitted in the formulas above.

Expression (8), valid for strong applied magnetic fields, can be rewritten analogously by introducing

$$a'^2 = \frac{B^2}{(B_{\text{DNP}\perp}^0)^2}, \quad c'^2 = \frac{\langle B_{f\parallel}^2 \rangle}{(B_{\text{DNP}\perp}^0)^2},$$

as

$$\rho \approx \frac{0.5(1 - e^{-t/\tau})^2 + c'^2}{a'^2 + (1 - e^{-t/\tau})^2 + 3c'^2} \quad (11)$$

and

$$\rho \approx \frac{0.5e^{-2t/\tau} + c'^2}{a'^2 + e^{-2t/\tau} + 3c'^2} \quad (12)$$

to describe the rise and decay of the transverse component of nuclear polarization, respectively.

In summary, using the expressions derived above, we can fit measured time-dependent degrees of polarization to evaluate nuclear spin relaxation times τ , as well as effective nuclear spin fluctuation fields and dynamic nuclear polarization. We note here that dynamics of the longitudinal and transverse components of nuclear polarization may be characterized by different relaxation times.

4.2. Dynamics of Nuclear Polarization Rise

Figures 4 and 5 show the results of an analysis of the time-dependent Hanle curves in Fig. 2, measured after the start of optical pumping. The values of ρ are refined by taking into account luminescence depolarization due to contributions from neutral quantum

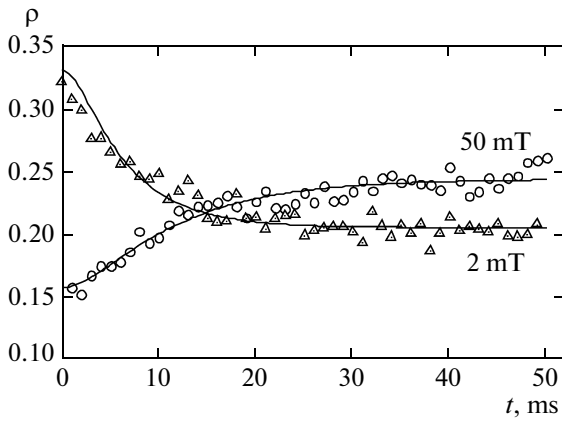


Fig. 4. Examples of time-dependent degree of polarization obtained by analyzing data presented in Fig. 2. Symbols represent experimental results for $B = 2$ and 50 mT; solid curves are approximations by functions (9) and (11).

dots. Experimental data were processed to determine the time-resolved degrees of polarization corresponding to several applied magnetic field strengths. Figure 4 demonstrates a wide difference between kinetics of degree of polarization under weak and strong field conditions (few milliteslas and higher than 20 mT, respectively).

At $B = 2$ mT (the lowest point of a dip in Fig. 3b, indicated by an arrow), where the dominant role is played by $B_{DNP\parallel}$, the degree of electron spin polarization ρ decreases with time elapsed (Fig. 4), signifying an increase in $B_{DNP\parallel}$ (see discussion in Section 3). We found that the time-dependent degree of polarization determined from experimental data can be fitted by (9) only if the transverse component of nuclear field is sufficiently weak, $B_{DNP\perp}^2 \ll \langle B_{f\parallel}^2 \rangle$. Using the resulting approximation, we estimated the characteristic rise time for $B_{DNP\parallel}$, $\tau_{\parallel} \approx 6$ ms, and the parameter $c = B_{DNP\parallel}^2 / \sqrt{\langle B_{f\parallel}^2 \rangle} \approx 1.5$.

Figure 4 shows an example of time-varying spin polarization found by processing experimental data obtained under high field conditions ($B = 50$ mT), where the dominant role is played by the transverse component of nuclear polarization. The solid curve is a fit by function (11). An analysis of the entire body of experimental data showed that all time-dependent spin polarizations measured at $B > 20$ mT are accurately approximated by this function. The parameters a' and c' calculated by fitting the polarization history for each applied magnetic field strength were then

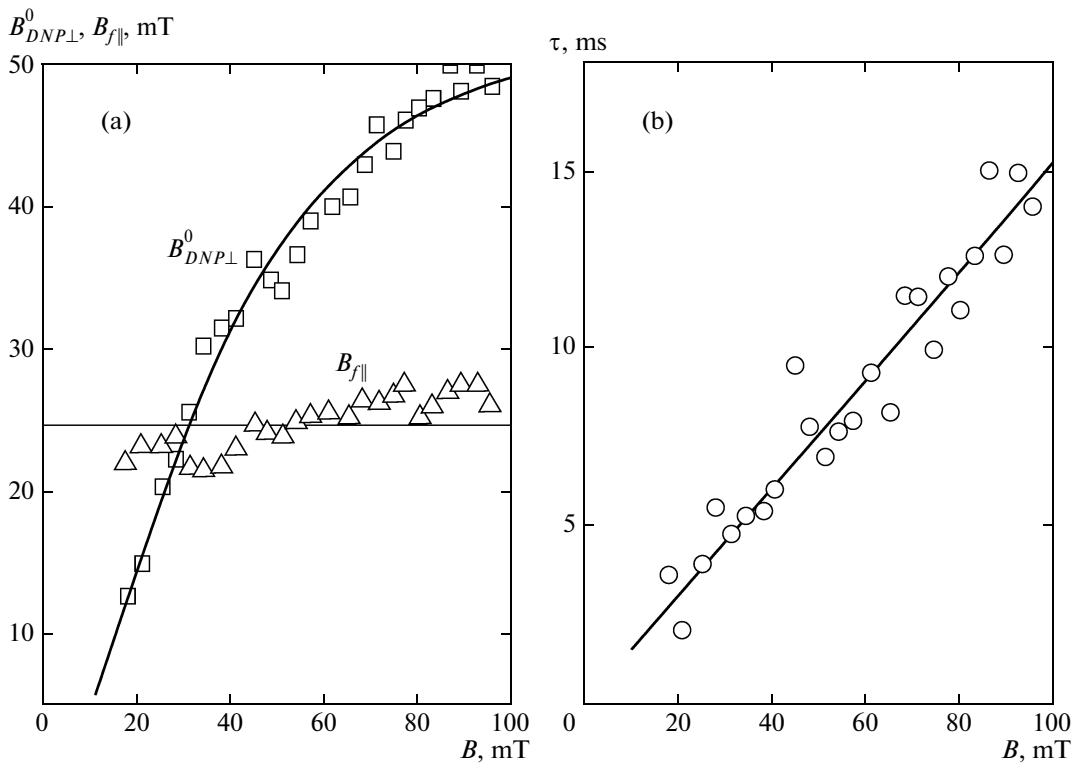


Fig. 5. (a) Limit magnitudes of the transverse nuclear field component $B_{DNP\perp}^0$ and the nuclear spin fluctuation field $B_{f\parallel}$ vs. applied field, obtained by analyzing kinetics of spin polarization after the start of pumping (see Fig. 2). (b) Field dependence of the buildup time τ of the transverse DNP field component. The solid curves are drawn for clarity.

used to determine the limit magnitude of the transverse component of nuclear polarization,

$$B_{\text{DNP}\perp}^0 = B/a',$$

the rms effective nuclear spin fluctuation field,

$$B_{f\parallel} \equiv \sqrt{\langle B_{f\parallel}^2 \rangle} = \frac{c'}{a} B,$$

and their dependence on magnetic field.

Figure 5a shows $B_{\text{DNP}\perp}^0$ and $B_{f\parallel}$ as functions of applied magnetic field. It is clear that the limit magnitude $B_{\text{DNP}\perp}^0$ of the transverse component of nuclear polarization increases approximately from 10 to 50 mT with an applied field between 20 and 100 mT, whereas the effective nuclear spin fluctuation field $B_{f\parallel}$ remains almost constant at around 25 mT irrespective of applied field strength. This value is in good agreement with data reported in [6], where the rms nuclear spin fluctuation field was estimated at approximately 20 mT for quantum dots of similar type. Using this value and $c \approx 1.5$ obtained above, we can also calculate the maximum transverse nuclear field: $B_{\text{DNP}\perp}^0 \approx 40$ mT.

Figure 5b shows the rise time τ of the transverse component of nuclear polarization. It demonstrates that the time linearly increases from approximately 2.5 to 15 ms with an applied field between 20 and 100 mT.

4.3. Dynamics of Nuclear Polarization Decay

An analogous procedure was used to analyze the shape of the Hanle curve as a function of dark time. Measurement results were converted into spin polarization kinetics for several values of applied magnetic field strength (as in Fig. 4), and the resulting curves were fitted by (10) and (12). The curves in Fig. 6 are examples of such fits. The fitting parameters were used to evaluate the initial longitudinal and transverse nuclear fields, as well as the corresponding decay times. The decay time of the longitudinal component $B_{\text{DNP}\parallel}^0$ calculated by using the data for $B = 2$ mT was found to be $\tau \approx 5.5$ ms, which is close to the corresponding rise time reported above.

However, the decay time of the transverse component $B_{\text{DNP}\perp}^0$ of nuclear polarization differs significantly from its rise time. Moreover, its time variation in an applied magnetic field exhibits an opposite trend: whereas the rise time increases with field strength (Fig. 5b), the decay time rapidly decreases (Fig. 7b). Accordingly, these times are approximately equal in strong magnetic fields but differ by a factor of several tens at $B = 20$ mT.

Remarkably, despite the difference in behavior between decay times, both the limit magnitudes of the DNP components and their variation with magnetic field in experiments on nuclear polarization decay are in good agreement with those determined by measur-

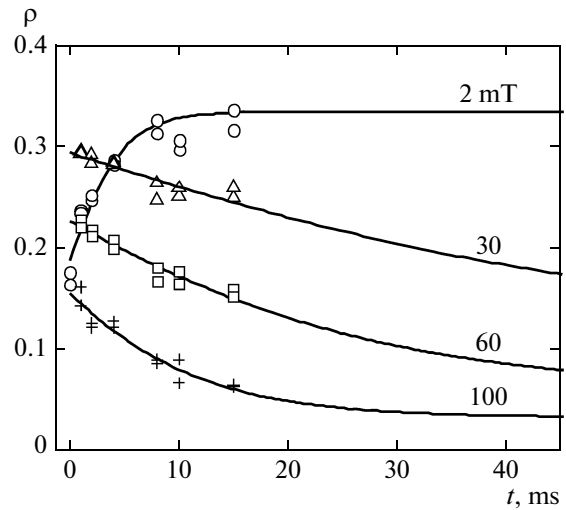


Fig. 6. Kinetics of degree of polarization at several magnetic field strengths (indicated at each curve), obtained by analyzing measurement results for various dark times. Symbols represent experimental data; solid curves are approximations by functions (10) and (12).

ing nuclear polarization buildup (cf. Figs. 5a and 7a).

The initial magnitude $B_{\text{DNP}\parallel}^0$ of the longitudinal component is approximately 30 mT, which is not too different from the limit magnitude of this component obtained in experiments on polarization buildup. A similar agreement is observed for the transverse component of nuclear polarization and the nuclear spin fluctuation field, as is clearly seen by comparing Figs. 5a and 7a. As in experiments on polarization rise, the initial magnitude $B_{\text{DNP}\perp}^0$ of transverse polarization increases with applied magnetic field, whereas the nuclear spin fluctuation field B_f is almost independent of applied field. A slight difference between nuclear field magnitudes measured in experiments on polarization buildup and decay should rather be attributed to a minor difference in optical excitation intensity between experiments of these two types.

5. DISCUSSION

Our analysis shows that the longitudinal and transverse components of nuclear polarization in the quantum dots under study exhibit widely different dynamical patterns. The behavior of longitudinal polarization is relatively simple. After the start of optical pumping, this component increases with a characteristic time of approximately 6 ms to a limit magnitude corresponding to an effective nuclear field of 30 to 40 mT. After the end of pumping, the longitudinal component decays over a similar time scale.

The behavior of the component of dynamic nuclear polarization perpendicular to the applied magnetic field is much more complicated. Observations that

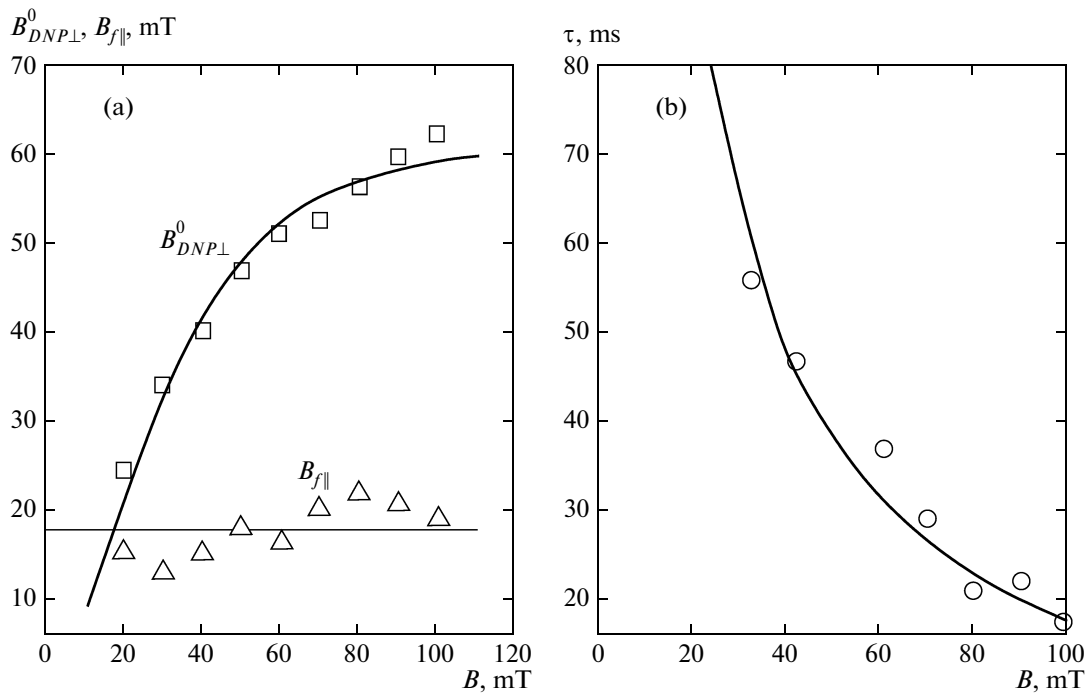


Fig. 7. (a) Field dependence of the initial magnitude $B_{DNP\perp}^0$ of the transverse nuclear field and the nuclear spin fluctuation field B_f , obtained by analyzing kinetics of spin polarization after the end of pumping (see Fig. 3). (b) Field dependence of the $B_{DNP\perp}^0$ decay time. The solid curves are drawn for clarity.

defy any straightforward explanation include difference between the buildup and decay times, their opposite variation with applied magnetic field, and increase in magnitude of this component with applied field strength.

In our view, these differences are mainly due to the fact that the dominant contributions to the buildup of longitudinal and transverse polarization components come from states with different spin projections on the viewing direction. Current models of nuclear polarization buildup are generally based on the classical model of angular momentum precession in isotropic space. The condition of spatial isotropy is violated in the quantum dots examined in this study because nuclei are affected by the field gradient due to the strain resulting from a mismatch between the lattice constants of the quantum dots and barrier layers. The principal axis of the field gradient is the structure growth axis, parallel to the viewing direction. The field gradient splits nuclear spin states into Kramers doublets $|\pm 1/2\rangle$, $|\pm 3/2\rangle$, etc. in indium, gallium, and arsenic nuclei, which have nonzero quadrupole moments. In an applied magnetic field, the Zeeman splitting in the doublets strongly depends on the relative orientation of gradient axis and magnetic field vector. This dependence can be described phenomenologically by introducing an anisotropic g -factor [19].

The anisotropy associated with the doublets $|\pm 1/2\rangle$ is relatively weak: the difference between the g -factor

components parallel and perpendicular to the gradient axis is not greater than a factor of 2 [16, 20]. Dynamics of these states should not be too different from the nuclear spin dynamics invoked to explain the W profile of the Hanle curve [9]. In the present study, one is naturally led to hypothesize that orientation of these particular states is responsible for the buildup of the component of nuclear polarization parallel to the applied field manifesting itself by the development of a W profile. This hypothesis is consistent with the relatively simple dynamical pattern of the longitudinal component of nuclear polarization observed in our experiments.

The g -factor anisotropy associated with the states $|\pm 3/2\rangle$, $|\pm 5/2\rangle$, ..., that are split off from $|\pm 1/2\rangle$ by quadrupole interaction is much stronger, as demonstrated in relatively weak magnetic fields. In a magnetic field parallel to the gradient axis, the splitting of these states linearly increases with field strength and the corresponding g -factor is similar to that in the absence of gradient. In a perpendicular magnetic field, the splitting is a highly nonlinear function of the field, and the g -factor (i.e., the splitting of these states) almost vanishes in fields on the order of a few milliteslas [16, 20]. In terms of the classical model, this means almost no precession of angular momenta associated with these states in a field of this kind. Suppression of precession impedes nuclear spin relaxation, which is generally attributed to local magnetic field

effects (e.g., see [21]). In effect, the transverse component of polarization of the nuclear states split off by quadrupole interactions can be stabilized to some degree in weak magnetic fields [11, 12]. A superlinear increase in splitting of these states with field strength enhances the probability of spin relaxation. The ensuing higher relaxation rate may be responsible for the shorter $B_{\text{DNP}\perp}$ decay times observed with increasing magnetic field strength in our experiments (see Fig. 7b).

Note the following counterintuitive observation: the time of nuclear polarization buildup after the start of pumping increases with applied field rather than decreasing (see Fig. 5b). To explain this behavior, we have to postulate that optical pumping gives rise to an additional process of $B_{\text{DNP}\perp}$ relaxation, whose rate in weak magnetic fields is several times higher than in darkness. The contribution of this process decreases with increasing magnetic field strength, and the buildup and decay times of $B_{\text{DNP}\perp}$ become almost equal in fields on the order of 100 mT. Furthermore, suppression of an additional relaxation process in strong magnetic fields explains the increase in limit magnitude $B_{\text{DNP}\perp}^0$ with increasing field strength (see Fig. 5a).

The nature of the additional relaxation process is currently unclear. It is likely due to interaction between nuclei and photoexcited carriers. This hypothesis is in good agreement with data reported in [5], where the presence of an electron in a quantum dot was shown to increase the rate of nuclear spin relaxation by more than two orders of magnitude.

This hypothesis is also corroborated by the results of our preliminary studies demonstrating that the relaxation time of nuclear spins in quantum dots increases by about two orders of magnitude after the sample has been annealed at a higher temperature of 980°C. Annealing increases the size of quantum dots, reducing the electron density around each nucleus.

6. CONCLUSIONS

We performed an experimental study of time-dependent circular polarization of luminescence from quantum dots as a function of magnetic field perpendicular to the optical axis (time-resolved measurements of the Hanle effect). Experimental data were analyzed by using an original approach to separate treatment of the longitudinal and transverse components of nuclear polarization in quantum dots characterized by strong quadrupole splitting of nuclear spin states. The phenomenological model proposed here takes into account the contribution of nuclear spin fluctuations, which were ignored in previous analyses of experimental data on the Hanle effect. The model is validated both by our finding that nuclear spin fluctuation field is independent of applied field and by good quantitative agreement with results of other studies [6,

18]. Using this model to analyze experimental results, we obtained detailed information about the rise and decay times of each component of nuclear polarization in quantum dots in a transverse magnetic field. The rise and decay times of the component parallel to the applied field were found to be almost equal (approximately 5 ms). However, the dynamics of the transverse component is much more complicated: the corresponding rise and decay times differ widely and have opposite dependence on magnetic field strength. Furthermore, the magnitude of the transverse component created by continuous-wave pumping significantly increases with applied field strength. We attribute this unexpected behavior of nuclear polarization to nuclear spin relaxation via interaction with photoexcited carriers.

ACKNOWLEDGMENTS

This work was supported by the Government of the Russian Federation, grant no. 11.G34.31.0067; the Russian Foundation for Basic Research, project no. 09-02-00482-a; Ministry of Education and Science of the Russian Federation, state contract no. 02.740.11.0244; and Deutsche Forschungsgemeinschaft Foundation.

REFERENCES

1. C. Jeffries, *Dynamic Nuclear Orientation* (Interscience, New York, 1963; Mir, Moscow, 1965).
2. *Optical Orientation*, Ed. by F. Meier and B. P. Zakharchenya (North-Holland, Amsterdam, 1984; Nauka, Leningrad, 1989).
3. V. K. Kalevich, K. V. Kavokin, and I. A. Merkulov, in *Spin Physics in Semiconductors*, Ed. by M. I. Dyakonov (Springer, Berlin, 2008), Chap. 11, p. 309.
4. V. K. Kalevich, V. D. Kul'kov, and V. G. Fleisher, *JETP Lett.* **35** (1), 20 (1982).
5. P. Maletinsky, A. Badolato, and A. Imamoglu, *Phys. Rev. Lett.* **99**, 056804 (2007).
6. R. V. Cherbunin, S. Yu. Verbin, T. Auer, D. R. Yakovlev, D. Reuter, A. D. Wieck, I. Ya. Gerlovin, I. V. Ignatiev, D. V. Vishnevsky, and M. Bayer, *Phys. Rev. B: Condens. Matter* **80**, 035326 (2009).
7. A. I. Tartakovskii, T. Wright, A. Russell, V. I. Fal'ko, A. B. Van'kov, J. Skiba-Szymanska, I. Drouzas, R. S. Kolodka, M. S. Skolnick, P. W. Fry, A. Tahraoui, H.-Y. Liu, and M. Hopkinson, *Phys. Rev. Lett.* **98**, 026806 (2007).
8. T. Belhadj, T. Kuroda, C.-M. Simon, T. Amand, T. Mano, K. Sakoda, N. Koguchi, X. Marie, and B. Urbaszek, *Phys. Rev. B: Condens. Matter* **78**, 205325 (2008).
9. D. Paget, G. Lampel, B. Sapoval, and V. I. Safarov, *Phys. Rev. B: Solid State* **15**, 5780 (1977).
10. O. Krebs, P. Maletinsky, T. Amand, B. Urbaszek, A. Lemaître, P. Voisin, X. Marie, and A. Imamoglu, *Phys. Rev. Lett.* **104**, 056603 (2010).

11. R. V. Cherbunin, S. Yu. Verbin, K. Flisinski, I. Ya. Gerlovin, I. V. Ignatiev, D. V. Vishnevsky, D. Reuter, A. D. Wieck, D. R. Yakovlev, and M. Bayer, *J. Phys.: Conf. Ser.* **245**, 012055 (2010).
12. R. I. Dzhioev and V. L. Korenev, *Phys. Rev. Lett.* **99**, 037401 (2007).
13. S. Cortez, O. Krebs, S. Laurent, M. Senes, X. Marie, P. Voisin, R. Ferreira, G. Bastard, J.-M. Gérard, and T. Amand, *Phys. Rev. Lett.* **89**, 207401 (2002).
14. A. Shabaev, E. A. Stina, A. S. Bracker, D. Gammon, A. L. Efros, V. L. Korenev, and I. Merkulov, *Phys. Rev. B: Condens. Matter* **79**, 035322 (2009).
15. I. V. Ignatiev, S. Yu. Verbin, I. Ya. Gerlovin, R. V. Cherbunin, and Y. Masumoto, *Opt. Spectrosc.* **106** (3), 375 (2009).
16. A. Abragam, *Principles of Nuclear Magnetism* (Oxford University Press, Oxford, 1961; Inostrannaya Literatura, Moscow, 1965).
17. I. A. Merkulov, A. L. Efros, and M. Rosen, *Phys. Rev. B: Condens. Matter* **65**, 205309 (2002).
18. M. Yu. Petrov, G. G. Kozlov, I. V. Ignatiev, R. V. Cherbunin, D. R. Yakovlev, and M. Bayer, *Phys. Rev. B: Condens. Matter* **80**, 125318 (2009).
19. E. S. Artemova and I. A. Merkulov, *Sov. Phys. Solid State* **27** (4), 694 (1985).
20. K. Flisinski, I. Ya. Gerlovin, I. V. Ignatiev, M. Yu. Petrov, S. Yu. Verbin, D. R. Yakovlev, and M. Bayer, *J. Phys.: Conf. Ser.* **245**, 012056 (2010).
21. M. I. D'yakonov and V. I. Perel', *Sov. Phys. JETP* **41** (4), 759 (1975).

Translated by A. Betev